IRANIAN JOURNAL OF PHYSICS RESEARCH

Iranian Journal of Physics Research, Vol. 6, No. 3, 2006

Signatures of granular superconductivity and Josephson effects in macroscopic measurements: the case of new superconductors

S Senoussi* and F Pesty

Laboratoire de Physique des Solides, associé au CNRS, Bât. 510, Université Paris-Sud 11, 91405 Orsay cedex, France
* Corresponding author: E-mail: senoussi@lps.u-psud.fr

(Received 26 June 2006; accepted 5 August 2006)

Abstract

We report systematic investigations of the magnetic superconducting properties of the new superconducting materials (NS): New high temperature superconductors (HTS), Organic superconductors (OS), fullerenes, carbon nanotubes, MgB_2 etc. We show that, contrary to conventional superconductors where the superconducting state can be coherent over several tenths of km, the macroscopic coherence range l_c of the NS is often as short as 0.1 to 10 μm typically. As a consequence, the magnetic properties are dominated by granular-like effects as well as Josephson coupling between grains. Here, we concentrate on HTS ceramics and organic superconductors exclusively. In the first case we observe three distinct regimes: (i) At very low field ($H < 5$ Oe to say) all the grains are coupled *via* Josephson effect and l_c can be considered as infinite. (2) At intermediate field ($5 < H < 50$ Oe, typically) the grains are gradually decoupled by H and/or T. (iii) At higher fields all the grains are decoupled and l_c roughly coincides with the diameter of the metallurgical grains. The case of OS is more subtle and is connected with a kind of order-disorder transition that occurs in most of them. For instance, in this study, we exploit quenched disorder (after crossing such a transition) in the κ-(BEDT-TTF)$_2$Cu[N(CN)$_2$]Br layered organic superconductor to get new insights on both the superconducting state ($T \leq 11.6$ K) and the glassy transition at T_g, by studying the superconducting properties as functions of annealing time and annealing temperature around the glassy transition. Our main result is that the data can be described by a percolation molecular cluster model in which the topology and the growth of the molecular clusters obey an Ising spin-glass-like model with $T_g \approx 80$ K for the hydrogenated compound and $T_g \approx 55$ K for the fully deuterated one.

Keywords: critical current, granular superconductivity, organic superconductors, glassy transition, streched expoenential, BEDT-TTF.

1. Introduction

Superconductivity was discovered in 1911 by H. Kamerling Onnes, of Leiden University, who observed that, when cooled to the helium liquid temperature (4.2K) the resistivity of mercury falls abruptly to zero. However, despite many efforts its microscopic origin remained misunderstood until the fifties. However a first important macroscopic theory was initiated by F. London and H. London in 1935, who modified Ohm's Law to obtain the Meissner effect,[1] without altering Maxwell's equations themselves. In their description [1] London brothers used the two-fluid model of Gorter and Casimir [2]. This macroscopic theory was then extended by Landau and Ginzburg in the more general theoretical frame of phase transitions. These macroscopic descriptions do not depend on the microscopic origin of superconductivity and are therefore always valid. In fact, the link between the Ginzburg-Landau equation and the microscopic parameters of superconductivity was established by Gor'kov over very general bases [3].

The microscopic origin of superconductivity and its quantum coherent nature was definitely demonstrated by John Bardeen, Leon Cooper, and John Schrieffer, the theory of whom is now known as the BCS theory). These theoretical developments gave rise to very intense experimental as well as theoretical researches during the sixties. Unfortunately, the enthusiasm rapidly declined and almost vanished during the early seventies. The reasons for such a decline is that until 1980 most solid state physicists, including some of the most renowned ones, thought that superconductivity was a property of metals and metallic alloys exclusively. More fundamentally, the same people believed that the superconducting transition temperature T_c will never exceed about 25-30K making potential industrial applications very limited. The first breakthrough in this widespread belief was the discovery of

1. Meissner effect refers to the fact that, below H_{c1} the superconductor excludes any magnetic field (whether external or induced by local super currents), except at the surface in a thin layer of thickness λ, the London penetration depth.

superconductivity in an organic conductor in 1980 by D. Jérome et al. [4], namely the now famous quasi-one-dimensional Bechgaard salt $(TMTSF)_2PF_6$ (T_c = 1.2K) synthesized in 1980 by Klaus Bechgaard of the University of Copenhagen. As it is well known, another very fundamental discovery that definitely turned upside down the situation was that of high temperature superconductors (HTS) by Müller and Bednorz [5] in 1986. Since then, an impressive number of organic as well as high-T_c superconductors have been identified, with T_c as high as 138 K for HTS and 15K for OS.

It is also worth mentioning that during the last few years superconductivity has been detected in a huge variety of exotic materials such as fullerenes [6] (fullerenes can also be considered as organic conductors, however for the sake of simplicity we will not discuss these materials anymore here), MgB_2 [7], carbon nanotubes [8,9] and other materials. Note that concerning nanotubes, the manifestation of superconductivity was somewhat indirect, *via* the so called "proximity effect" and is still a controversial subject, at least as magnetic measurements are concerned [10]. Indeed, according to Tang et al. [10] single-walled 4-Angström diameter carbon nanotubes embedded in a zeolite matrix revealed a superconducting transition temperature of 15 K. Moreover, the authors claim that statistical mechanics calculations based on the Ginzburg-Landau free-energy functional yield predictions that are in excellent agreement with their results. Nevertheless, to the best of our knowledge, these results have never been reproduced in any research group including the authors themselves.[2]

At this point we note a further significant difference between conventional and most of the new superconductors. For conventional low-T superconductors the superconducting state is in general macroscopically coherent even for polycrystalline materials. For instance, in a typical high field superconducting commercial magnet (made of Nb_3Sn with T_c =18.1 K) the superconducting state may be coherent over several tenths km which corresponds to the whole length of the superconducting wire composing the coil magnet. On the contrary, most of the new superconductors, including all those enumerated above, behave like granular superconductors when prepared by standard "metallurgical techniques". Here, the word granular means that in some experimental conditions (that will be clarified latter) the coherence length is much smaller than the macroscopic radius R of the sample and sometimes of the order of, or less than, the London penetration depth λ (λ = 0.1 to 1 μm typically). This has several enormous experimental consequences: (1) One consequence is the inevitable presence of Josephson junctions (often called weak links in granular materials) between adjacent coherent grains, the manifestation of which will critically depend on the experimental conditions. (2) Another consequence (with which we are very interested here) concerns Meissner effect which tends to vanish as the grain size r_g becomes smaller than the London penetration depth. For instance, a direct experimental implication of this size effect is the fact that strictly one dimensional (1D) superconductors are impossible to investigate and therefore to detect by magnetic measurements. The reason for this is quite simple. The magnetic moment of a superconductor sample always results from closed super-current loops within the sample. However, closed loops are by definition impossible to produce in 1D materials. Another way to express this 1D property is to say that λ is infinite for field penetration along the non-conducting directions of the 1D material.

Clearly, it is their granular nature that limits the technical and industrial applications of the new superconducting materials. Indeed, as just noted, the grain boundaries behave like weak links limiting the inter-granular critical current density $J_{c,inter}$ (which is equivalent to the transport critical current density, $J_{c,tr}$) to a few 10^3 A/cm^2. This is a very small value as compared with the intra-grain critical current density $J_{c,intra}$ which can be as high as 10^7A/cm^2 in HTS samples. In addition, the inter-granular current is extremely sensitive to any magnetic field (this is at the origin of the term "weak link") and is generally suppressed by a field of a few tenths of Oe or less: It can be said that the Josephson second critical field $H_{J,c2}$ characterizing granular superconductors is typically four to five orders of magnitudes smaller than H_{c2} of the bulk. What is very interesting and intriguing is that the situation is quite different in conventional low temperature superconductors (LTS) where the grain boundaries do not behave like weak links and thus do not play such a negative role for $J_{c,tr}$.

For the sake of technical applications, it may be interesting to ask the question why such a difference between conventional and new superconductors. Some of the reasons for this difference could be: (1) the physics of SNS (metallic alloys) and SIS junctions (HTS and probably SO materials) are quite different (Remind that SNS means Superconductor–Metal–Superconductor junction while SIS refer to Superconductor–Insulator–Superconductor junction). (2) The grain boundaries are generally much cleaner and better defined in metals and metallic alloys than in new superconductors. (3) Perhaps more fundamentally, in conventional superconductors the thickness of the grain boundary is generally much smaller than the coherence length ξ.

Considering again the concept of granular superconductivity, we must emphasize that the effective

2. According to our estimate based on (i) the size effect (r/λ ratio), (ii) the 1D nature of their carbon nanotubes and (iii) the relatively high magnetic field used in their measurements (up to 5 Teslas) we estimate that, even if we accept that their material is really superconducting, the magnetic data reported by the authors are at least 10^7 (seven orders of magnitude) larger than expected from our calculation. In other words, we claim that, even if it exists really, superconductivity is impossible to detect by such magnetic measurements in such single walled nanotubes. In fact, we believe these results as unphysical.

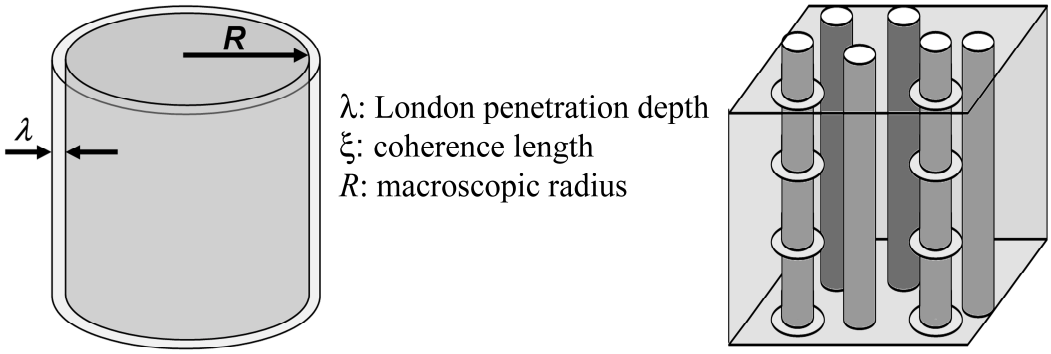

Figure 1. Microscopic field penetration in a perfect 3D type II superconductor. Left $H < H_{c1}$: an ideal superconducting material expels the magnetic field except near the surface in a thin shell of depth λ. In usual conditions the sample radius R is much larger than λ and one considers that the magnetic shielding (or Meissner effect) is perfect. Right $H > H_{c1}$: The field penetrates the sample in the form of quantized vortices. In an ideal 3D material the vortices form a perfect triangular lattice.

superconducting grains do not necessarily coincide with the usual "metallurgical grains", especially for OS where the "granular superconductivity" seems to always exist even in perfect single crystals (for instance, as determined by X ray observations at room temperatures). This exotic granularity is in fact induced by a kind of order-disorder transition at low temperature (see hereafter for more details on this transformation).

The outline of this paper is as follows: Firstly, we will remind the theoretical aspects of granular superconductivity that are of interest for the present study. Secondly, these theoretical predictions will be illustrated by some experimental results in HTC superconductors. Thirdly, we will then concentrate on the magnetic properties of the 2D κ-(BEDT-TTF)$_2$X organic superconductors. Contrary to the 1D Bechgaard salts, these are quasi-two-dimensional and superconducting at ambient pressure and not too low temperatures, 8-12K, facilitating their investigations by magnetic measurements.

Finally, we feel from the above discussion that the role of size effects in the interpretation of the experimental data is much more important in the new superconductors than in conventional ones. This is why we will devote much attention to this aspect here.

2. The equilibrium magnetization, M_{eq}, of superconducting materials

It is probable that magnetic measurements represent the most powerful experimental technique not only for standard characterization but also for the most fundamental investigations of superconducting materials. In addition, usual magnetic experiments are relatively easy and within reach of practically any solid state physicist. However, very often the quantitative interpretation of the data is another story. This is why we will insist here very much on these interpretations. For this purpose, we will first distinguish between (1) the so-called equilibrium magnetization M_{eq} (i.e., the magnetization of perfect defect-free superconducting materials) and (2) the so-called irreversible magnetization M_{ir} induced by defects. The latter is related to vortex pinning and vortex creep. At this point, it is important to emphasize that, even when the defects concentration is very low (less than 1% to say), M_{ir} is not necessarily a small perturbation of M_{eq} but instead it can exceeds M_{eq} by several orders of magnitudes. Another very important question to always bear in mind when interpreting the experimental data concerns the interplay between the macroscopic shape of "the visible sample" and other, possibly hidden, semi-macroscopic structures, such as granular effects, especially when the grain radius r_g is comparable or smaller than λ.

2. 1 M_{eq} of 3D superconductors of size much larger than λ.

We have just noticed that the investigation of the magnetization provides important information on the most fundamental parameters of the superconducting state (namely, J_c, H_{c1}, H_{c2}, λ and ξ). Before discussing some behaviors more typical of layered superconductors, let us first recall the expressions of M_{eq} for ideal three-dimensional type II superconductors in the limit $R \rightarrow \infty$ (we remind that R is the macroscopic radius of the sample, generally much larger than λ while r or r_g refer to small grains)

The equilibrium magnetization of such type II superconductors has first been calculated by Abrikosov [11, 12, 13, 14] who predicted the appearance of vortices in the mixed state defined by $H > H_{c1}$. In this mixed state, M_{eq} is controlled by a repulsive vortex-vortex interaction that determines the number of vortices within the material as well as the symmetry of the vortex lattice. figure 1 illustrates the flux and current distributions (microscopic representation) in the Meissner phase ($H < H_{c1}$, Figure 1, left,) and in the mixed or Abrikosov's state ($H > H_{c1}$, Figure 1, right) in which the field penetrates the sample in the form of vortices.

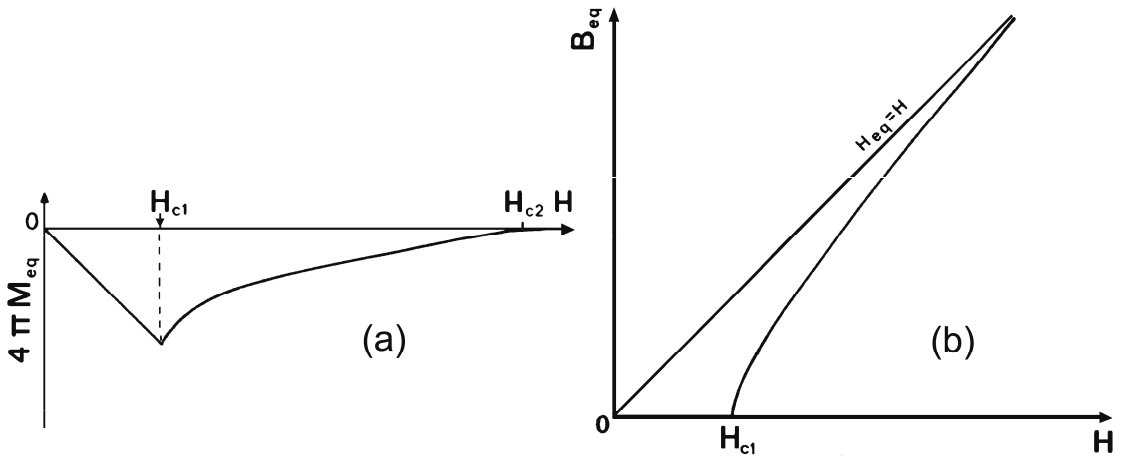

Figure 2. (a) Schematic representation of the equilibrium magnetization of type II superconductors. (b) The associated magnetic induction $B(H)$ (for $T << T_c$). We see that B=0 for $H < H_{c1}$, traducing the Meissner effect. Keep in mind that $B(H)$ is related to $M_{eq}(H)$ through Eqs. 1 to 5 and that the demagnetizing field is equal to zero here ($N = 0$).

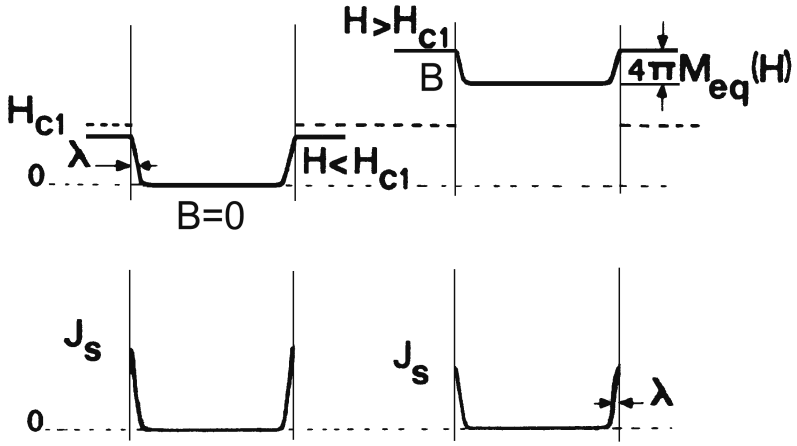

Figure 3. Macroscopic profiles of the local induction $B(r)$ (a) and the associated reversible surface currents (b), in a cylindrical sample of a perfect type II material, for $H < H_{c1}$ (left side) and $H \geq H_{c1}$ (right side).

In its first version, Abrikosov's theory considers an ideal isotropic material with no size effects, no surface barriers, and negligible thermal fluctuations in the vortex lattice. Bear in mind however that most of these effects are not negligible in real experiments and must be considered when analyzing the data.

Abrikosov's $M_{eq}(H)$ and the associated $B(H)$ curves are presented schematically in figure 2a and figure 2b respectively. We see that $B = 0$ for $H < H_{c1}$, expressing the usual Meissner effect (i.e., perfect shielding)

To help understanding the physical meaning of the equilibrium magnetization, we also show in figure 3 the macroscopic distribution of fields (top) and currents within the material at equilibrium (bottom). Note that this distribution is the same as in figure 1 but is more appropriated for the analysis of macroscopic measurements.

At this point it is important to remind that the measured magnetization is entirely due to the surface current flowing around the sample, as sketched in figure 3. *In other terms, a perfect superconductor cannot carry any current in its volume except near its surface in a thin shell of depth equal to* λ. *This is why a perfect superconductor is of no many uses for technical and industrial applications.*

To understand the field and current profiles sketched in figure 3 we must remind that H and B are related to M_{eq} by Gauss equation $B - H = 4\pi M_{eq}(H,T)$ and to the total current I by Ampere's theorem, assuming that the sample is a very long cylinder of length L with zero demagnetizing field, so that the effective field is equal to H outside the sample, and to B inside it. Then, Ampere's theorem gives $B - H = I/L = 4\pi M_{eq}$.

Now we come back to figure 2-3 and write the theoretical $M_{eq}(H)$ as calculated by Abrikosov in the so-called London approximation [11-14]. The theoretical $M_{eq}(H)$ curve has an infinite slope at $H = H_{c1}$ (Figure 2) while it varies extremely slowly (logarithmically) with H for $H >> H_{c_1}$. Neglecting again demagnetizing effects we have:

$$M_{eq}(H,T) = -\frac{H}{4\pi} \qquad (H < H_{c1}), \tag{1}$$

$$4\pi\left[\frac{\partial M_{eq}}{\partial H}\right]_{H-H_{c1}\to 0^+} = \infty \qquad (H - H_{c1} \to 0^+), \tag{2}$$

$$4\pi\left[\frac{\partial M_{eq}}{\partial H}\right]_{H_{c2}>>H>>H_{c1}} = \frac{-H_{c1}}{2H\ln(\kappa)}, \tag{3}$$

$$with \quad H_{c1} = \frac{\Phi_o \ln(\kappa)}{4\pi\lambda^2}, \tag{4}$$

$$4\pi\left[\frac{\partial M_{eq}}{\partial H}\right]_{H\to H_{c2}} = \frac{-H_{c2}}{(2\kappa^2 - 1)\beta}, \tag{5}$$

Here $\kappa = \lambda/\xi$ while β is a parameter of the order of (or slightly greater than) unity.

We have already noted that more general theories [15,16] show that at fields lower than the thermodynamic field these expressions can be notably modified by surface barriers. Other theoretical treatments by Z. Hao et al. [17, 18] account more rigorously for vortex core effects, particularly near the critical field H_{c2}. For instance, the contribution of the currents circulating very close to the vortex cores transforms eqs. 3 and 4 into:

$$M_{eq} = -\beta(H,T)\frac{\Phi_o \ln(\kappa)}{16\pi^2\lambda^2}\ln\left[\alpha(H,T)\frac{H}{H_{c2}}\right], \quad (H >> H_{c1}) \tag{6}$$

Here $\alpha(H,T)$ and $\beta(H,T)$ are fitting parameters (close to unity) that slowly vary with field and temperature (approximate values valid in restricted field domains are given in Ref. [18]).

2. 2 Influence of the demagnetizing factor *N* on M_{eq}

We know that the experimental magnetization depends on the external shape of the sample through the usual demagnetizing factor *N* and through the field penetration depth. The influence of ordinary demagnetizing field is illustrated in figure 4, for various values of *N* (corresponding to a well defined elliptical shape) and for a more realistic case (inset) with a distribution of *N* such that $\langle N \rangle = 0.6$ (average value) and $\Delta N = 0.1$. The dashed curve of the inset corresponds to $N = 0.6$ and $\Delta N = 0$. One sees that any distribution in *N* suppresses the anomaly in M_{eq} at $H = H_{c1}$. One also sees how the demagnetizing effects increase the effective field seen by the sample and displace the apparent H_{c1} towards lower values.

2. 3 Influence of the effective size of the sample on M_{eq} through the λ / r ratio

We have seen that in the usual London model the equilibrium magnetization is produced by surface-like currents circulating around the sample within the London penetration depth λ. This implies that the above eqs. 1 to 6 giving M_{eq} cease to be valid when the size of the effective sample – or the scale of the defect structure – becomes comparable with or smaller than λ. At this point we note that λ diverges at T_c, making the condition $\lambda > R$ always true close enough to the superconducting transition.

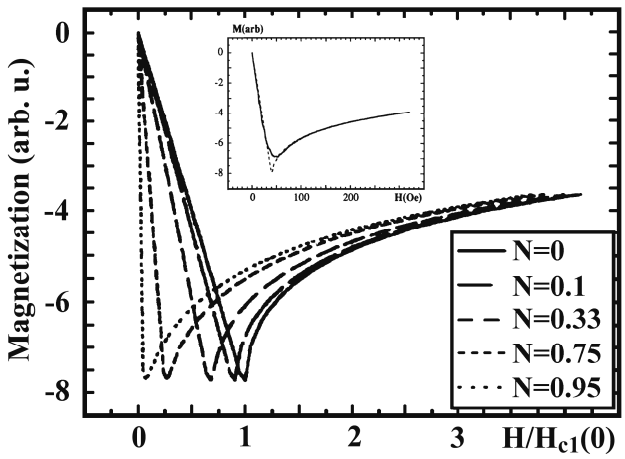

Figure 4. Equilibrium magnetization as a function of *H* for five different demagnetizing factors indicated in the figure. Note the logarithmic anomaly at $H=H_{c1}$. Inset: The continuous curve represents M_{eq} for a more realistic example characterized by a normal distribution of *N* such that $N = 0.6$ (average value) and $\Delta N = 0.1$. The dashed curve of the inset also corresponds to $N = 0.6$ but with $\Delta N = 0$.

The influence of the factor λ/R on M_{eq} has been first calculated by London for a spherical specimen [1] and then by Clem for a cylindrical shape with *H* parallel to the cylinder axis [19] and for $H < H_{c1}$ (see also Senoussi [20] and eqs. 5-7, pages 38-39 of Ref. [21]). eqs. 7-9 below are the results of such calculations. These equations can be applied to the individual grains of granular materials if Josephson and dipolar couplings are both negligible.

$$M_{eq} = -\frac{3H}{8\pi}\left[1 - 3\frac{\lambda}{r}\coth\left(\frac{r}{\lambda}\right) + 3\left(\frac{\lambda}{r}\right)^2\right] \text{ (sphere)} \tag{7}$$

$$M_{eq} = -\frac{H}{4\pi}\left[1 - \exp\left(-\frac{r}{\lambda}\right)\right] \text{(slab)} \tag{8}$$

$$M_{eq,ll} = -\frac{H}{4\pi}\left[1 - 2\frac{I_1(r/\lambda)}{I_0(r/\lambda)}\right] \text{ (}H\text{ parallel to the cylinder axis)} \tag{9}$$

$$M_{eq,\perp} = -\frac{H}{2\pi}\left[1 - 2\frac{I_1(r/\lambda)}{I_0(r/\lambda)}\right] \text{ (}H\text{ perpendicular to the cylinder axis)} \tag{10}$$

Here $I_1(x)$ *and* $I_o(x)$ are the modified Bessel functions of the first kind, of order one and zero respectively. *H* is parallel to the surfaces of the slab (eq. 8) and to the cylinder axis in eq. 9. It is perpendicular to the cylinder axis for eq. 10. For the sake of simplicity we will also assume that the temperature dependence of λ obeys the phenomenological two-fluid model:

$$\lambda = \lambda(0,0)\left[1 - \left(\frac{T}{T_c}\right)^4\right]^{-1/2} \tag{11}$$

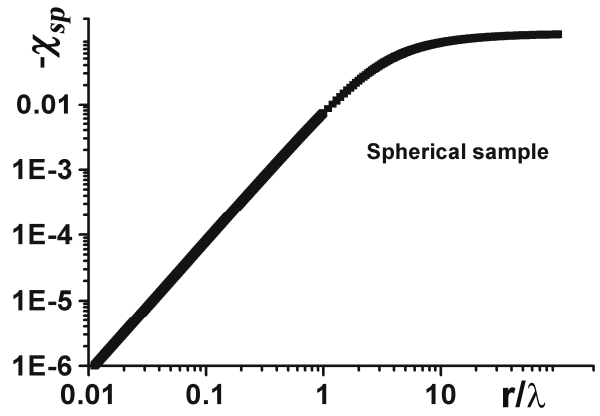

Figure 5. Calculated magnetic susceptibility (eq. 13) as a function of the ratio r/λ for a spherical sample (sp) and for $H < H_{c1}$ (the first critical field).

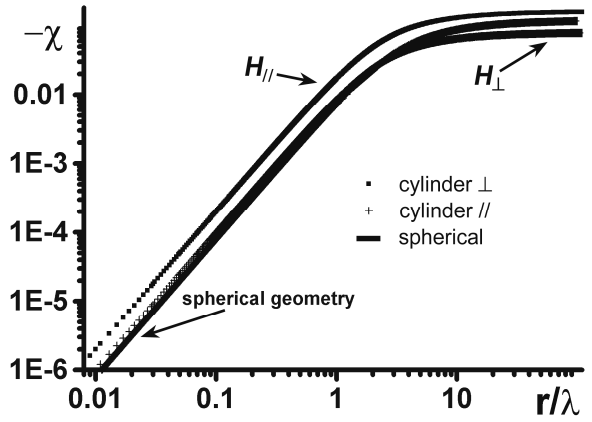

Figure 6. Compares the magnetic susceptibility ($H < H_{c1}$) as a function of the ratio r/λ of a spherical sample and a cylindrical sample with $H_{//}$ (H_{para}) and $H_{\perp}$ (H_{per}) to the cylinder axis, respectively.

In figure 5 we show the calculated magnetic susceptibility $\chi_{sp} = M_{eq}/H$ (based on eq. 7) as a function of the ratio r/λ in log–log scales for a spherical grain. We clearly see that χ_{sp} starts to fall off abruptly for $r < \lambda$.

In figure 6 we compare the calculated χ for three different geometries: spherical (eq. 7), cylindrical with H either parallel (H_{paral}) or perpendicular (H_{per}) to the cylinder axis (eqs. 8 and 10, respectively) as a function of the same r/λ ratio. We see in figure 6 that the evolution of χ with r/λ does not depend very much on the exact geometry of the grain. This means that the interpretation of the experimental results does not depend rigorously on the exact shape of the grains.

In figure 7 we plot the magnetic susceptibility of a spherical sample, (eq. 7) as a function of temperature for various r/λ (0) ratios indicated on the figure. Here, λ is assumed to vary following the classical phenomenological two-fluid model (eq. 11). Note also that, to facilitate the comparison with experimental results, we take T_c approximately equal to that of the organic superconductor that will be investigated later.

Figure 7 assumes that, (1) the spherical grain is perfect (i.e., the grain has a perfect crystalline form) and (2) the condition $H \leq H_{c1}$ is always realized. Of course, both conditions are only valid in certain experimental conditions that have to be clarified now: (1) Since $H_{c1}(T) \rightarrow 0$ when $T \rightarrow T_c$, this means that as T approaches T_c there is necessarily a crossover temperature T_{cr} at which $H = H_{c1}(T_{cr})$.

Using the temperature dependence of $H_{c1}(T)$ (see eqs. 4 and 11) and equating H to $H_{c1}(T)$ we find (remind that N is the demagnetizing factor) :

$$T_{cr} \approx T_c\left[1-\frac{H}{(1-N)H_{c1}(0)}\right]^{1/4} \approx T_c\left[1-\frac{H}{4(1-N)H_{c1}(0)}\right], \quad R >> \lambda(T),\ H << H_{c1}(0). \qquad (12)$$

Above this temperature the variation of the measured magnetic susceptibility ceases to be independent of the applied field and becomes in fact very complicated as a function of this field. More precisely: $\chi = M_{eq}/H$ is now governed by equations of the form given in eqs. 2-6 instead of Eq. 1. Nevertheless, in many ac susceptibility experiments one has $H << H_{c1}(0)$, then T_{cr} is very close to T_c and can be ignored.

3. The irreversible magnetization of superconducting materials

In real materials there are intra-grain imperfections (not accounted for in any of the above descriptions) that pin the vortex lines, whether Josephson or Abrikosov's vortices. This adds a non-equilibrium term, M_{ir}, to the measured magnetic signal. Contrary to M_{eq} which is induced by surface currents (flowing in the London penetration depth) M_{ir} is induced by currents circulating inside the volume of the specimen. It is such currents in the volume that define the critical current density. For the sake of simplicity one usually considers that the critical current density is homogeneous through the specimen *and only depends on the local magnetic field.* However, we remind that the main object of the present paper is to show that this is not justified in the presence of very extended defects as in the case of sintered HTS, organic superconductors, nanotubes, etc. Let us first remind Bean's model, which ignores such extended inhomogeneities.

3. 1 The Bean's critical state

To relate the irreversible magnetization to the field and current profiles inside the specimen, Bean [22] assumed that the critical current density can only take one value among three different states J_c, $-J_c$ or zero, depending on the electromagnetic history of the sample. Moreover, Bean's model neglects time effects (especially flux creep) in the magnetization (except possibly those imposed by Maxwell equations during variations of the external fields). The hysteresis cycle together with the field and current profiles determined from this model are illustrated in figure 8 (see figure caption for more details).

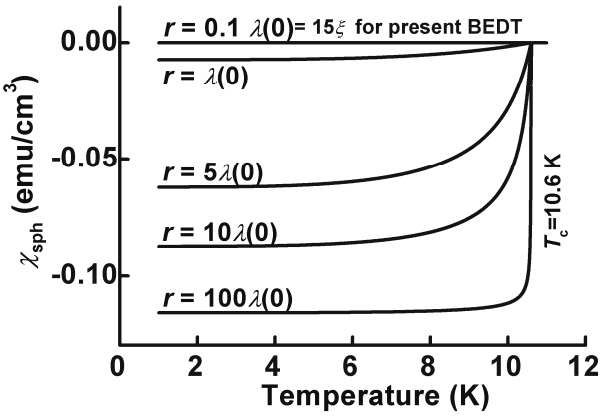

Figure 7. Plot of the magnetic susceptibility of a ideal spherical sample as a function of temperature for the indicated r/λ ratios (see eqs. 13 and 17). The data are based on the two-fluid model and are valid in the limit $H \to 0$ or as long as $H \leq H_{c1}$.

Bean's model is particularly useful for $H > H_p$, where H_p is the field limit above which the sample is entirely penetrated by magnetic flux, i.e., down to its core. Under the above conditions the critical current density is related to the hysteresis cycle by the eqs. 13-16 below. Note that in these equations R is in cm, J_c in A/cm^2 and M in emu/cm^3 ("practical units of Bean" obtained from CGS units by replacing c, the velocity of light, by 10), valid for a fully penetrated cylindrical sample with H perpendicular to the basal plane one has:

$$J_c = 15\ \frac{M^+ - M^-}{R} = 30\ \frac{M_{ir}}{R}, \qquad (13)$$

Here M^+ and M^- refer to the upper and lower branches of the hysteresis cycle, respectively. For a rectangular or ellipsoidal sample with dimensions a and b in the basal plane ($a > b$ and H perpendicular to this plane), the Bean equation takes the form:

$$J_c = 30\ \frac{M_{ir}}{b}\ \frac{2}{3 - b/a}. \qquad (14)$$

Usually, one also uses the hysteresis cycle to define M_{rev} and M_{ir} as follows:

$$M_{rev} = \frac{M^+ + M^-}{2}, \qquad (15)$$

$$M_{ir} = \frac{M^+ - M^-}{2}. \qquad (16)$$

The determination of the hysteresis cycle, particularly the associated eq. 15, is straightforward. We indeed remind that the measured magnetization is the sum of all the magnetic dipoles $S(r)dI$ induced by all the elementary current loops within the sample (dI is the elementary current while S is the area of the loop). In other words the magnetization by unit volume $M_{ir} = \sum S(r)\, dI/V$ (SI units) where $V = \pi L R^2$ is the volume of the sample. Here $dI = J_c L dr$ is the elementary current of the loop of area $S = \pi r^2$. Let $H < H_p = J_c R$ and $r^* = R(1\text{-}h)$ (see Figure 8 for the $r^*(H)$ relationship). Then we can rewrite:

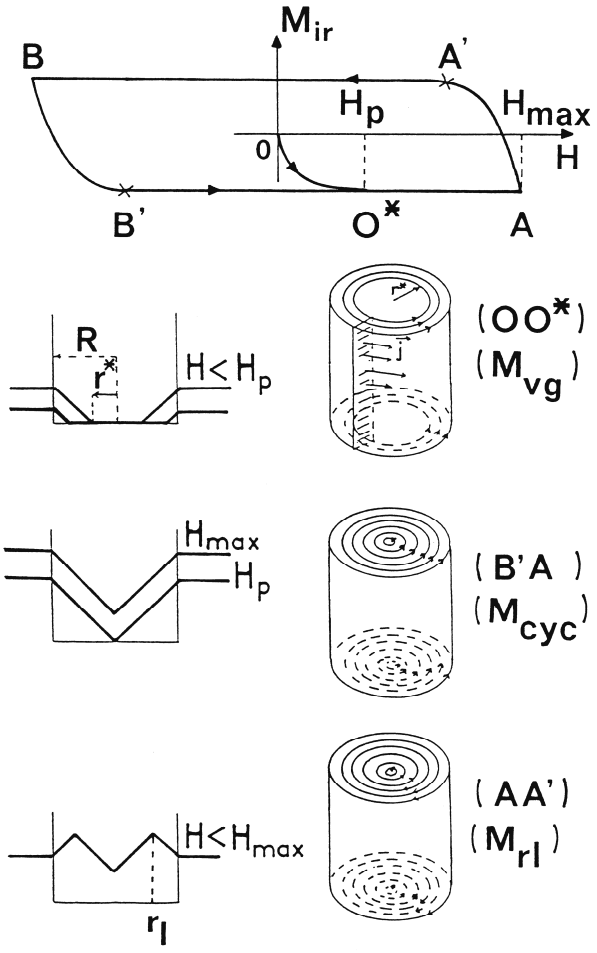

Figure 8. (a) Schematic definition of the various branches of the hysteresis cycle (based on the Bean model) of a hard type II superconductor. OO* is the "virgin" or "initial" magnetization. A'B and B'A define the "cyclic critical" state whereas BB' and AA' refer to "reversal" states. Also shown is the field H_p at which magnetic flux just reaches the center of the specimen (assumed to be cylindrical). The lower figures represent the field and current profiles associated with the various branches of the cycle, in particular the virgin magnetization M_{vg} ($H < H_p$). As in the usual Bean model M_{eq} is taken equal to zero (but see Senoussi et al. [20, 23]) and J_c is assumed to be independent of both H and r, except via the magnetic history.

$$M_{ir} = \frac{1}{L\pi R^2}\int_{r^*}^{R} L J_c \pi r^2 dr = \frac{J_c R}{3}\left(1 - r'^3\right) = \frac{J_c R}{3}\left(3h - 3h^2 + h^3\right), \qquad (17)$$

here, $h = H/H_p < 1$, $H_p = J_c R$, *and* $r' = r/R = 1 - h$

$$M_{ir} = \frac{J_c R}{3} \quad \textit{for } h > 1, \quad \textit{(SI units, or } \frac{J_c R}{30} \textit{ in practical units of Bean)} \qquad (18)$$

We remind that the above figure 8 and the associated formulae 15-18 of the Bean model assume a homogeneous (coherent) cylindrical sample in which the

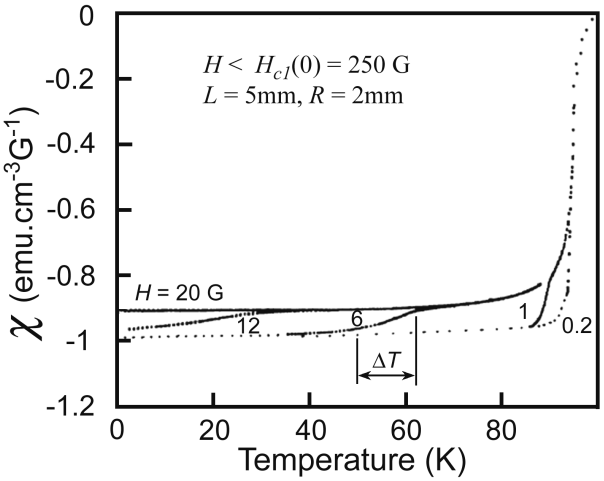

Figure 9. This graph displays the magnetic susceptibility of a sintered YBCO as a function of temperature at different fixed fields. The grains size is of order 10 μm. One clearly see the coherent limit and the incoherent-granular limits defined by two envelops. The steps correspond to the passage from the coherent to the incoherent behavior.

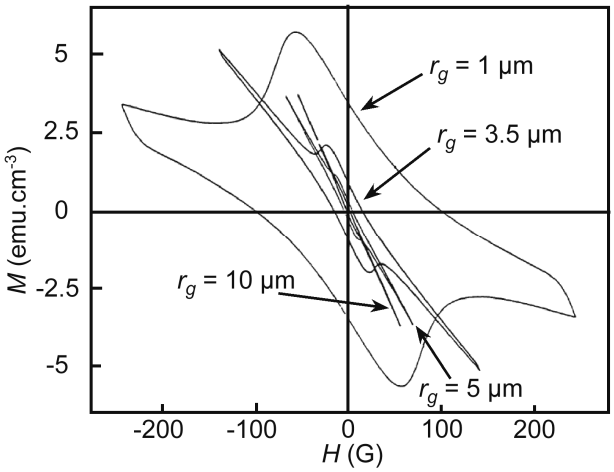

Figure 10. Low field hysteresis cycles for 4 different grain sizes (1 to 10 μm). These tiny cycles are typical of ceramic HTS and are signatures of Josephson junctions. The initial slopes are roughly the same for the four samples, but after the suppression of the junctions by the applied field, the slope then decreases with *r*.

critical current density does not depend explicitly either on *r* or on *H*. The Bean model is very useful to investigate the critical current density and other physics of the vortex lattice. Unfortunately, very often this model cannot be applied in its usual form just described. It is the experimentalist's job to determine when this Bean model can be applied and when a more elaborated granular description is more appropriated. In the following paragraphs we will present examples of such granular situations.

4. Experimental results in HTS ceramics

In real experiments the crystalline structure is generally very inhomogeneous and the hysteresis cycle as well as the superconducting transition crucially depends on such a defect structure. This influence is generally extremely complicated however, to facilitate the interpretation, it can be classified into the following two limiting cases.

On the one hand, small defects of size comparable to ξ or less embedded in a perfect superconducting medium generally improve the superconducting transition, (i.e., make it more abrupt at least below the so-called irreversibility line). A further and more fundamental benefit of small defects is that they are very efficient to pin vortices and therefore to improve the critical current density, especially in as prepared materials.

On the other hand, extended-connected defects can behave like weak links (or Josephson junctions) and generally broaden the superconducting transition. They also considerably degrade the effective (or transport) critical current density, since this current will be limited by the weak links. Of course, we are here more interested in the latter case since grain boundaries can be considered as connected defects.

In figures 9-11 we present the experimental magnetization of sintered superconducting $YBa_2Cu_3O_7$ as a function of the ceramic grain radius. The question is then under which experimental conditions can we apply the above granular analysis (Figure 5-8 and associated eqs. 13-27) to real macroscopic though granular samples? In real conditions the grains can be coupled together, especially at very low *H* and very low *T*, through two different interaction mechanisms. The first one is the very common dipolar interaction that is at the origin of demagnetizing effects exemplified by the curves in figure 4. Since dipolar interaction is of long range it always exists. Fortunately, as it is of long range it can simply be described (to a first approximation) by the macroscopic demagnetizing factor *N* of the macroscopic sample, thus ignoring the internal granular structure [23]. The second interaction with which we are more concerned here is the Josephson coupling between adjacent grains. As it is well known, Josephson coupling is extremely sensitive to both field *H* and temperature *T*, as well as to the thickness *d* of the junction. This is why, up to now, Josephson junctions considerably limit the industrial applications of HTS materials. This coupling-decoupling effect is well illustrated in figure 9-11 below which we analyze now.

4.1 Manifestation of granularity as well as Josephson junctions in the magnetic susceptibility of sintered $YBa_2Cu_3O_7$.

Figure 9 shows the magnetic susceptibility as a function of temperature at various fixed fields (varying from 0.2 to 20 Oe) for a very compact sintered $YBa_2Cu_3O_7$ granular samples. Clearly, the curves do not resemble any of those displayed in figure 7.

We indeed clearly see two limiting envelops. One (dashed curve) corresponds to the limit $H \to 0$. This envelop defines in fact the coherent behavior where all

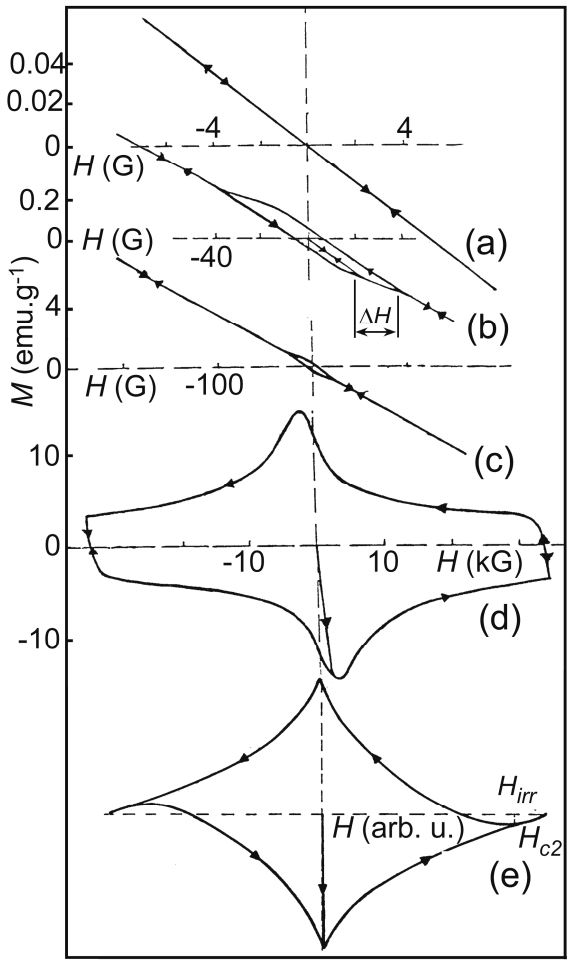

Figure 11. Examples of magnetization loops of sintered granular superconductors at increasing field scales (a, b, c, d) extending from $H < H_{c1}^{w}$ *to* $H > H_{ir}$. Here H_{c1}^{w} *and* H_{ir} are the weak link (or Josephson) first critical field and the irreversibility field, respectively (e) Schematic variation of M in the depinning line region. This example is typical of the ceramic $YBa_2Cu_3O_7$. At very low H, M is linear, reversible, and exhibits perfect screening if $R >> \lambda_{wl}$ (the Josephson penetration depth in the weak links). As we will discuss it later this behavior should be common for organic superconductors, however it should be very difficult to observe here, because the Josephson fields and currents as well as the transition temperature are much lower and, more fundamentally, much more distributed in these materials.

the grains are coupled together *via* Josephson mechanism, so that the sample appears like a single superconducting grain. In other words, in this limit all of the junctions are on. The other envelop (upper solid curve) defines the incoherent behavior above which all the grains are fully decoupled (off). It is this envelop that gives information on the size of the superconducting grains as compared to λ. The steps between the two envelops represent the gradual destruction of the Josephson junctions by temperature for the indicated fixed applied field. The width of the steps measures the statistical distribution of the junction thickness (even though a large contribution to this broadening arises from the pinning of Josephson vortices)

4. 2 Manifestation of granularity and Josephson junctions in the hysteresis cycle of sintered $YBa_2Cu_3O_7$.

Figure 10 shows the low-field hysteresis cycles (T=4.2 K and H<250 Oe $\approx H_{c1}(0)$) for four sintered –granular YBCO samples of the same macroscopic shape but differing by the average grain sizes : $r_g \approx$ 1, 3.5, 5 and 10 μ m. Since the applied field is smaller than the bulk first critical field, the tiny hysteresis cycle cannot be ascribed to Abrikosov's vortices but is necessarily due to the pinning of Josephson vortices by junction imperfections. Examining figure 10 we note that:

- The initial slope is the same for the four samples. Since by definition the initial slope is the magnetic susceptibility χ_i, this result is consistent with our previous interpretation of figure 9 that as $H \rightarrow 0$ all the grains are coupled together, and the magnetic response is imposed by the macroscopic shape of the material alone (coherent limit).
- The final slope χ_f varies approximately like $1/r_g$. Again this is consistent with our granular analysis (see eq. 10 for example) and the interpretation of the upper envelop of figure 9.
- Here too, the steps indicate the gradual suppression of the Josephson junctions, by the magnetic field (instead of temperature as in figure 9).
- The area of the cycle is proportional to the number of Josephson junctions
- The width of the cycle ($\Delta M = M^{+}\text{-}M^{-} = 2M_{ir}$) is proportional to the transport critical current density but in a more subtle way than predicted in Bean's model. More precisely, J_{tr} and ΔM are now approximately related by $J_{tr} = [15\ \Delta M/r_g] \times [\chi_i / \chi_i \text{-} \chi_f)]$: There is an additional factor $\chi_i / \chi_i \text{-} \chi_f)$ that corrects for the fact that the width of the cycle is proportional to the number of junctions crossed by the current loops (in the coherent state) while the critical current is a single junction propertiy.
- Like in figure 9, the width of the steps gives information on the thickness statistical distribution of the junctions.

4. 3 The transition from Josephson's low field hysteresis cycle to Abrikosov's high field hysteresis cycle

So far we have limited our experimental results to the case $H << H_{c1}$ where the magnetic signal is imposed by London surface currents and/or by Josephson currents exclusively. Now we wish to extend our discussion to the case $H > H_{c1}$ when the field start to penetrate into the grains in the form of Abrikosov's vortices. As already noticed, these Abrikosov vortices can be pinned by small defects giving rise to a irreversible magnetization as well as increased critical current density. This is illustrated in figure 11 that shows the hysteresis cycle of a sintered granular YBCO at different field scales, extending from $H << H_{c1}$ to $H >> H_{c1}$ [24].

Like in figure 10 above we observe (figure 11a,b,c)

the appearance of a low-field irreversibility regime at $H << H_{c1}$ (It is to be emphasized that this low field regime does not exist in single crystal materials). What is also very interesting here is the appearance of a high field irreversibility regime (figure 11d,e) which is well separated from the low field one. This implies that the statistical distribution in the physical properties of the Josephson junctions (which are at the origin of the tiny cycle) is very narrow. The same kind of behavior is observed in all other HTS materials. This is not true for organic superconductors, which we wish to examine now.

5. Experimental results in organic superconductors: Topological spin glass-like clustering

It is known [25-34] that the organic conductor κ-(BEDT-TTF)$_2$Cu[N(CN)$_2$]Br, – where BEDT-TTF is the bis (ethylenedithio) tetra-thiafulvalenium molecule while Cu[N(CN)$_2$]Br is a monovalent anion – undergoes a structural transition (also called "glassy transition") at a certain temperature (T_g = 70–80 K) and becomes superconductor below about 12 K. Moreover, in some circumstances this material exhibits a magnetic transition around 10–20 K preceded by the onset of magnetic fluctuations at about 50 K [35, 36].

Typically, T_g is about one order of magnitude higher than the superconducting transition T_c. For the present example of κ-(BEDT-TTF)$_2$Cu[N(CN)$_2$]Br, T_c is about 11.6 K while T_g is order 80 K for the hydrogenated compound. It is also well known that organic superconductors generally present strong deviations from perfect shielding (i.e., $-4\pi(1\text{-N})\chi << 1$), correlated with incomplete "annealing" of the sample upon cooling through the order–disorder transition.

In most cases these deviations have been interpreted as a direct measure of the so-called fractional superconducting volume v_s, neglecting any possible granular effects. The present authors [37] were the first to show that this classical interpretation is generally wrong and that organic superconductors exhibit a granular-like behavior with χ strongly controlled by the factor r/λ. Of course, the exact granular structure and the associated Josephson network would depend somehow on the microscopic nature of the order-disorder transition itself. Our idea was the following: by analogy with other phase transitions, it is expected that when the sample is cooled through this transition the ordered state would nucleate simultaneously at many different points of the material.

Firstly, this would lead to a multi-domain structure in which the individual domains grow up with the annealing time (or as the inverse of the cooling rate) near the transformation temperature T_g (here, 80 K).

Secondly, it is expected that these annealing times control the size of both the superconducting domains (as well as the strength of the Josephson coupling between them) and the junction network.

Thirdly, the exact spatial structure (or the topology) of the domains and the associated Josephson junctions network would reflect the exact nature of the transition.

Fourthly, this topology could be inferred from macroscopic measurements (transport and magnetic) in the superconducting state. Before considering our experimental data, let us first remind some of the known properties of the 80 K transformation.

5. 1 The molecular origin of the 80 K transformation in κ-(BEDT-TTF)$_2$Cu[N(CN)$_2$]Br

Let us now remind some known properties of the order-disorder transition (hereafter called the 80 K anomaly) in κ-(BEDT-TTF)$_2$Cu[N(CN)$_2$]Br. At first, we note that there is a consensus among organic superconductor specialists (see Tanatar et al. [26 , 27] and references therein) that this transformation is associated with a gradual ordering-freezing of the ethylene groups at the ends of the BEDT-TTF molecules. More precisely, at higher temperature the ethylene groups rapidly oscillate between two different conformations. Upon cooling, these thermal fluctuations gradually slow down. Simultaneously, a kind of long-range order among the ethylene groups builds up by choosing one from the two conformations (so-called: "staggered" or "eclipsed").

However, we emphasize that the low-temperature state contains some amount of quenched disorder that strongly depends on the anion species (Cu[N(CN)$_2$]Br$^-$ here), the applied pressure, the cooling conditions and, more importantly, on whether the ethylene groups are formed by hydrogen bonds (denoted H8-Br) or deuterium bonds (denoted D8-Br). This is why the exact nature of the 80 K anomaly and the associated low-temperature superconducting state are still not understood. For instance, D8-Br exhibits several puzzling superconducting properties. Some of these properties were ascribed to the appearance of a magnetic transition at low temperature (10-20 K), the meaning of which is unclear. Several mechanisms have been proposed including spin-density waves, [38] spin canting, [36] or the suppression of superconductivity by dispersed magnetic ions associated with the persistent disorder [39]. Also, some authors [31, 32, 40] ascribed the decrease of the apparent superconducting volume to an increase in λ (the in-plane penetration depth) through mean-free-path effect. [31]. However none of these mechanisms is able to explain, even qualitatively, the experimental data reported below:

1) The fact that the apparent magnetic current density j_c always decreases (instead of increasing if one accepts the usual models) as the degree of quenched disorder increases. 2) The low-field susceptibility also decreases in the same experimental conditions. For instance, if one accepts such interpretations one is led to assume that λ can reach unphysical values, as high as 0.1 mm [32] (and much more if applied to our present results). 3) Despite these large changes in the apparent j_c and the apparent λ, T_c stays almost constant. 4) As the quenched disorder is increased one observes several unusual phenomena:

firstly, the appearance of increasing irreversibilities at $H << H_{c1}$ (remind that for coherent superconductors we expect no hysteresis below H_{c1}), secondly, a large broadening of the superconducting transition. Instead, the experimental data and the theoretical analysis we present below prove that all of these features can naturally be explained in the framework of a granular model and the associated weak links connecting the grains. In addition the spatial structure of the grains is similar to that of spin clusters in an Ising spin glass.

5. 2 Experimental data and analysis

We have investigated the ac magnetic susceptibility and the dc magnetization of the superconducting phase after performing a series of thermal treatments on a D8-Br single-crystal of dimension ~ 1 × 1 × 0.25 mm^3. To this end, we annealed the sample inside the SQUID cryostat at different fixed temperatures T_a ranging from 65 to 110 K. Moreover, in order to carefully monitor the development of ethylene ordering as a function of time at a given T_a, we varied the cumulated annealing time t_a from about 30 seconds at 100 K to about 2 × 10^6 sec at 65 K. At each T_a the cumulated time t_a was divided into a sequence of intervals (say Δt_w) ranging from about 20 seconds at 95 K to 12 hours at 65 K. At the end of each interval Δt_w the sample was rapidly cooled (20 K/min) to 2K. The ac susceptibility $\chi(T)$ (ac field $h = 3$ Oe) and the magnetic hysteresis cycle $M_i(H)$ ($0 < H < 1000$ Oe, typically) were subsequently measured between 2 and 15 K using a Quantum Design SQUID. Then, the sample was again rapidly warmed up (10 K/min) to the same T_a, after which the same annealing-cooling-measuring procedure was repeated. Note that the fastest cooling rate was limited by the cooling power of the SQUID and yielded a systematic error in the origin of the annealing time. However, we found this to be negligible below about 85 K.

As inferred from the data below, we find that the only way to explain the experimental results is the cluster-like description.

Figure 12 shows both the in-phase ($4\pi\chi$, lower plots) and the normalized out-of-phase (χ", upper plots) ac susceptibilities as functions of temperature (2-15 K) for t_a ranging from about 0 to 7260 minutes and for $T_a = 69$ K. Taking into account the demagnetizing factor for our parallelepiped geometry, $N \approx 0.65$ [41] we find $-4\pi\chi(1-N) \approx 0.84$ for the longest annealing time. Diamagnetic shielding is still below its maximum possible value, defined by $-4\pi\chi(1-N)=1$. However, the missing 16% are accounted for by the fact that the ratio r/λ is not infinite. Indeed, an exact calculation for spherical particles with a ratio r/λ of about 20 fully explains the difference.

Considering again the χ curves we observe a large broadening of the superconducting transition, especially for the most rapidly cooled cases. In addition, as illustrated by the imaginary susceptibility χ" (upper panel), this broadening is accompanied by significant magnetic losses (remind that χ" is proportional to such losses), particularly for short annealing times. Then, since for homogeneous systems we expect negligible hysteresis for measuring fields smaller than the first critical field $H_{c1} \approx 20$ Oe, [42] the most plausible explanation for such hysteresis effects would be the presence of weak links between adjacent clusters, with a large distribution of the associated Josephson critical fields [20] The observed broadening is not necessarily due to inhomogeneities in the temperature transition T_c but can principally be explained by the following mechanisms inherent to any cluster model. Firstly, it is known that when $\lambda(T) >> r$, χ varies as $(\lambda/r)^2$ [20, 43]. Then, since r is widely distributed and tends to zero with very short annealing time, this yields a natural broadening that can be defined by the condition $\lambda(T) > r$. A second source of broadening is connected with the distribution and the temperature dependence of the Josephson critical fields [20, 44], which is expected to be very large for spin-glass-like clustering. Thirdly, we also expect strong variations in T_c when r becomes comparable with the bulk coherence length ξ. However, for strong type II superconductors as it is the case here ($\kappa = \lambda/\xi > 140$, $\lambda \approx 0.7\,\mu m$, Ref. [42]), isolated clusters of such sizes are hard to detect in standard magnetic measurements.

Figure 13 displays M_i vs. H curves obtained at 2 K after following the same annealing procedures as in figure 12 (M_p denotes the magnetization at the peak of a cycle.) Here too, we observe a gradual improvement in M_i with t_a. In addition, from the H-dependence of the M_i curves, we deduce that the pinning strength also increases with t_a. The inset to figure 13 is an expansion of the low-H cycle for two representative annealing times: $t_a \approx 5$ and 1800 minutes (note the difference of about 18 in vertical scales). Obviously, the low-H behavior of the most annealed state (filled symbols) is perfectly reversible (to within the experimental limit) and linear, while that of the quenched state (open symbols) exhibits strong irreversibilities even at H as low as 1 Oe. For the same physical reasons as for χ, the presence of hysteresis reflects the increasing role of weak links at short annealing times. The increase in the pinning energy with t_a can also be explained by the gradual reduction of the number of such weak links with increasing t_a. Finally, all these results confirm that the superconducting clusters and the non superconducting ones are highly entangled.

We now present in figure 14 the ac susceptibility χ together with the peak magnetization M_p as functions of the annealing time at 72, 69 and 65 K. Let us first focus on the 69 and 72 curves from which we draw the following four properties. 1) The relaxation is more rapid for χ than for M_p. 2) Both χ and M_p tend toward saturation. From now on we shall call these saturation limits M_s and χ_s. 3) χ_s is nearly the same for 72 and

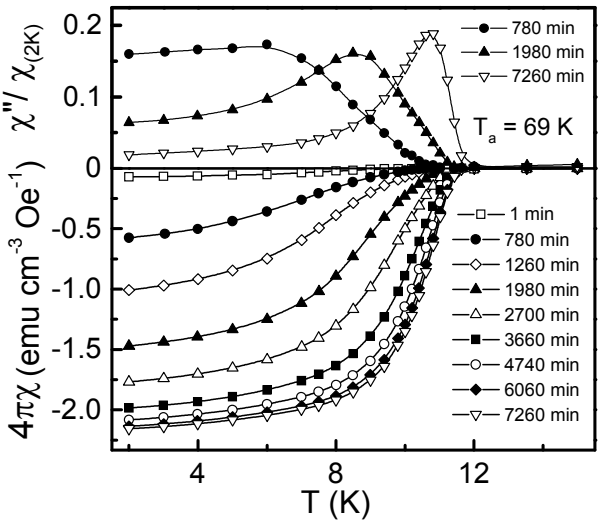

Figure 12. In-phase (χ , lower part) and out-of-phase (χ'' in relative units, upper part) ac susceptibilities of deuterated κ-(BEDT-TTF)$_2$Cu[N(CN)$_2$]Br vs. temperature (h = 3 Oe), plotted after annealing then quenching (from T_a = 69 K) as described by the labels in the figure. For the sake of clarity, only half of the registered curves is displayed. The solid lines are guides to the eyes.

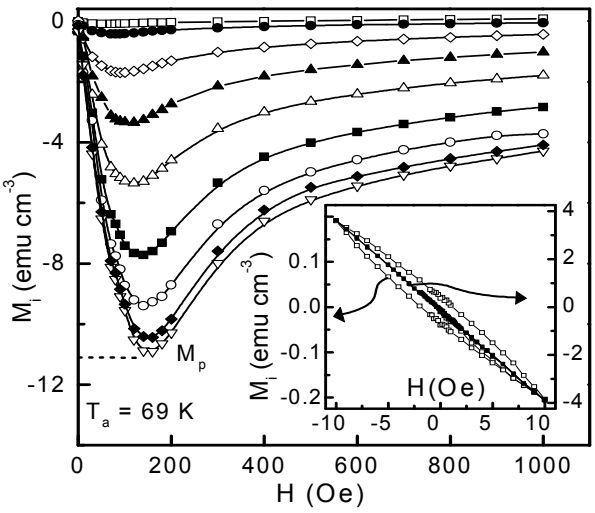

Figure 13. Magnetization M_i vs. H, measured at 2 K, after the same heat treatment (and same symbols) as in figure 12. The peak magnetization is denoted M_p. The solid lines are guides to the eyes. The inset is an expansion of M_i near $H = 0$ for $t_a \approx 0$ (left scale) and t_a = 7260 min (right). Note the difference of 18 in the vertical scales.

69 K while M_s changes by a factor of almost two. 4) More fundamentally, these saturation values are found to be reproducible and independent of the previous thermal history (see inset to figure 14). This suggests that they correspond to an equilibrium thermodynamic state.

The examination of the 69 K curves reveals that both χ and M_p follow two consecutive regimes as functions of t_a. Firstly, an initial time regime, described by a power law. Such a regime is preponderant below 66 K, but becomes practically inaccessible above T_a = 72 K (because of the finite cooling-heating rates). It is spectacularly illustrated by the 65 K curves, which also reveal a considerable slowing down of the relaxation rates below about 69 K. Secondly, a long time regime described by a stretched exponential law $\propto \left(1 - \exp\left(-(t/\tau)^{\beta}\right)\right)$ (represented by solid lines on the M_p curves). It corresponds to the saturation limit just discussed. This regime is dominant above 72 K but out of reach experimentally below 63-64 K (as it needs a t_a of several years).

Such a two-regime behavior is common in many fields of physics and is known as "growth and coalescence". In spin glasses the short time regime is associated with a "fine-grained structure" while the long time one, called α regime, defines the single exponential and the stretched exponential regimes [45, 46, 47]. Considering the long time regime, we find $\beta \approx 1$ for $T \geq 69$ K and $\beta \approx 0.5 \pm 0.1$ at 66 K (note that the fitting functions are shown as solid lines for M_p and dashed lines for χ).

Figure 15 shows the variation against T_a of both M_s and χ_S , calculated by extrapolating the fitting curves as

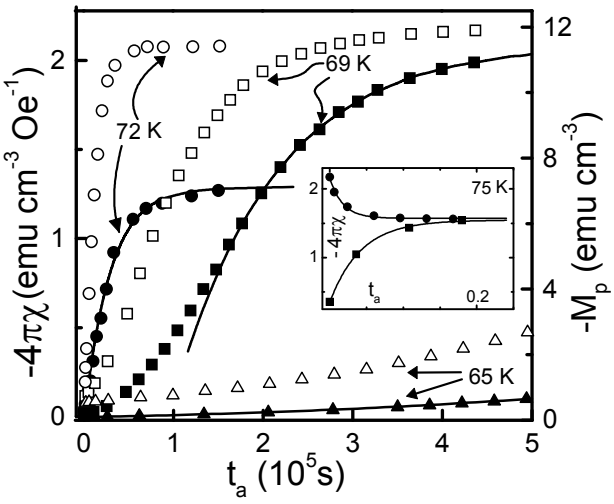

Figure 14. Peak magnetization M_p (filled symbols, right scale) and susceptibility χ (open symbols, left scale) at 2 K vs. annealing time at T_a = 65 (triangles), 69 (squares) and 72 K (circles). Note that above 69 K both quantities tend to saturate but more rapidly for χ . The inset shows that the relaxed state does not depend on whether this state is reached from below or above its saturation value. The solid lines represent fitting curves (see text). The asymptotic values deduced from fitting are called M_s and χ_S .

explained before. We see again that the two quantities vary quite differently with decreasing T_a: below 70 K, χ_S tends toward a plateau whereas M_s increases more and more rapidly. This reflects an anomalous increase in the cluster size as T_a decreases and confirms further the cluster description. Indeed, the length scales are very different for the two quantities: χ_S is expected to

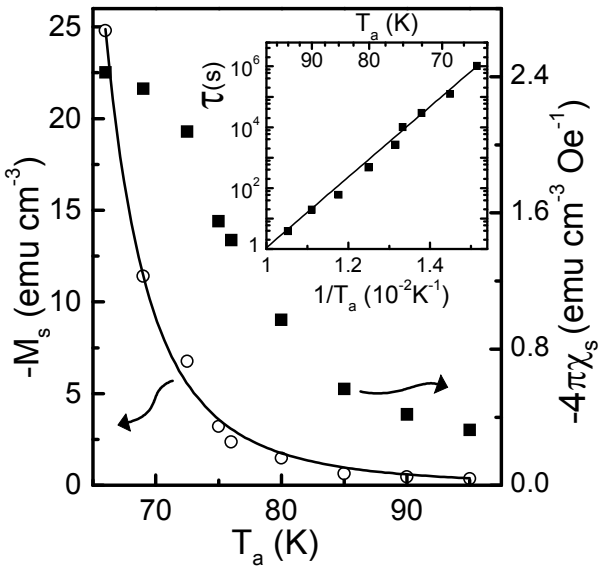

Figure 15. Saturation values M_s and χ_S as functions of annealing temperature T_a. As illustrated by the solid line, M_s follows a scaling law (see text). The inset is a semi logarithmic plot of the relaxation time as a function of $1/T_a$: the fitting function (solid line) is a stretched exponential with $\beta \approx 1$ for $T_a > 69$ K and $\beta \approx 0.5 \pm 0.1$ at 66 K (see text).

saturate for $r >> \lambda \approx 0.7\,\mu m$ while M_s would continue increasing up to $r \approx R \approx 500\ \mu m$ (Bean's model, see below). Moreover, we are able to fit M_s with a scaling law of the form $M_s = M_0 \left(T/T_g - 1\right)^{-n}$ (continuous line in figure 15) with $T_g \approx 55$ K, $n \approx 3.2$ and $M_0 \approx 0.16$ emu cm^{-3}. The inset shows the long time relaxation τ (associated with M_i) as a function of T_a in a semi-logarithmic scale. The data fit remarkably well with an Arrhenius function $\tau(T) = \tau_0 \exp(U/T)$ with an activation energy U of about 2660 K and an attempt frequency $1/\tau_0$ of about 2×10^{13} s^{-1}. Our U value is in excellent agreement with NMR data [35, 36] at 200-350 K and to a lesser extent with resistivity measurements [28]. However, our results differ qualitatively and quantitatively from other transport data [26]. Combining the NMR frequencies reported in Refs. [35, 36] and our time scale shows that the $\exp(U/T)$ law is obeyed over 15 orders of magnitude. By contrast our attempt frequency is two orders of magnitudes smaller than that deduced from NMR. However, we have experimental evidence that this difference is a mere isotopic effect. In most publications on the subject, the interpretation of susceptibility measurements were based on the classical Meissner formula: $4\pi(1\text{-}N)\ \chi = (v_s/v_{ech})$ for $T \to 0$. Remind that v_s is the superconducting volume while $v_{ech} = v_s + v_n$ is the total volume of the sample with v_n being the normal (or possibly insulating) volume. In the same way, usually, the irreversible magnetization M_i and the associated J_c are assumed to be related by Bean's model $M_i = v_S \times R \times J_c / 30$, where R is the macroscopic radius of the sample. These formulae implicitly neglect any granular and any weak link effects.

As a matter of fact, if one tries to interpret our data in such a picture, one is led to unphysical values for both λ and J_c (i.e., λ could be as high as 1 cm and J_c as low as 100 A/cm^2). In addition, such a model can explain neither the low-H irreversibility nor the transition broadening. Actually, our data are consistent with a granular interpretation where the macroscopic radius R must be substituted by some average cluster radius r. Moreover, the topology of the clusters can be described by a percolation model [45] and/or a Ising spin-glass-like model [46] according to which the cluster size grows as $\left\langle r^2 \right\rangle \approx C\left(1 - \exp\left(-(t/\tau)^{\beta}\right)\right)$. Here τ and β depend on the dimensionality of the material and on the treatment temperature. The model predicts that as T is lowered, β would vary from ≤ 1 at $T \geq T_p$ to 1/3 at $T << T_p$ (stretched exponential) where $T_p > T_g$ is the percolation threshold temperature. Our data are consistent with $\beta \approx 1$ at $T \geq 69$ K and $\beta = 0.5 \pm 0.1$ at 66 K. In fact, we observe a dramatic slowing down of τ for $T \leq 66$ K suggesting that T_p is close to this temperature. Moreover, as predicted by the spin glass model [46, 47] we observe that this slowing down is accompanied by the onset of a two relaxation regime. Accepting again the analogy with spin glasses, our data suggest the presence of two critical points T_p and T_g, corresponding to a percolation threshold and to a true thermodynamic transition [48], respectively. At this point, it is worth noting that the deduced T_g, of about 55 K, lies in the temperature range where ferromagnetic fluctuations take place, while the resistivity behavior changes from semi-conducting to metallic. Using a granular analysis [20, 43, 44], we find that at equilibrium r varies from about 0.1 μm at $T_a \approx 100$ K to 10–30 μm at 66 K.

Finally, the present results prove clearly that the superconducting properties are determined by the quenched disorder created while crossing the glass transition and not by a possible onset of magnetic effects below this transition. The analogy with spin-glasses is straightforward: like Ising spins, ethylene molecules have only two allowed states. In addition, the canonical RKKW interactions can be simulated by a random distribution of incommensurate CDWs [49, 50]. Nevertheless, more theoretical developments are needed to better describe the glassy transition.

Another remarkable work on temporal processes in the resistivity of a high purity κ-(BEDT-TTF)$_2$Cu[N(CN)$_2$]Br single crystal can be found in Ref. [28]. See also Refs. [25, 26, 27] for other resistivity data.

6. Conclusion

In this paper we concentrated on granular superconductivity and its manifestation in experimental

results. We have seen that in most examples of the literature the reduction of the diamagnetic signal often observed in new superconductors has generally been ascribed to a diminution of the superconducting volume fraction that would be equal to the deviation from perfect shielding. Following the analysis outlined above, we suggest this is generally incorrect unless there are evidences that the fractional superconducting volume is imposed by very large (larger than λ) and unconnected defects.

We have indeed seen that for a multi-domain – or granular – structure, in which the grain boundaries are multi-connected, the shielding factor strongly decreases with the ratio λ/r, even when the thickness d of the junctions is very small, i.e., even when the true superconducting volume v_s is close to one. The superconducting transition near T_c has also been measured by a number of authors, some of them having found a substantial broadening of the transition and thus strong deviations from the London approximation. In many cases these deviations have been ascribed to thermal fluctuations. This is very convincing for some very good samples but, as discussed above, it is also possible that some of these deviations – especially at fields smaller than $H_{c1}(0)$ – come from structural inhomogeneities in the material, for instance those induced by the order–disorder transition in organic conductors.

Concerning the critical current density, the situation becomes to be clarified since the distinction between intra- and inter-grain current densities is now quite well understood, at least for very low T and H (The situation is still very complicated and interesting near T_c).

Concerning organic superconductors the results of the literature considerably vary from one author to another and the granular aspects are not yet accepted by many specialists in this field. As discussed above we believe that the main cause of such confusions is again the 80-K transformation and the associated domain-like structure. As already discussed, the latter introduces an effective domain radius in Bean's model, which can be much smaller than the macroscopic radius. As a result, we know very little concerning the pinning properties of organic superconductors. As compared to HTS, the difficulty here lies in the fact that the statistical distribution of the Josephson parameters, including Josephson currents, is extremely large because of the fractal spin-glass-like nature of the Josephson-junctions network. New investigations with the 80 K transformation in mind are needed. Therefore, it will be very interesting to extend the present measurements and analysis to other organic superconductors. It will be also very interesting to apply the same annealing-cooling-warming procedures to the transport properties and try to correlate these properties in the superconducting and in the normal phases.

From our analysis we propose that when the magnetic shielding is imperfect (after correcting for the demagnetizing field) it is generally more correct to consider the sample as multi-domain-like rather than being made of a single superconducting domain, and to determine the characteristic size of the grains from the experimental data.

We have discussed and sometimes established the optimum conditions to interpret the experimental data and determine the important physical parameters such as V_s (the true fractional volume), J_c and λ.

Finally, we can apply the same analysis to carbon nanotubes, the superconducting properties of which are not clear though they have been the focus of considerable research activity in recent years.

It is clear from all the above discussions and results that organic superconductors offer a unique opportunity to study (and perhaps to distinguish between) the contributions of various physical defects and thermal fluctuations to the broadening of the superconducting transition around T_c. These materials also offer a vast (still almost virgin) field to study the pinning properties of the vortex lattice.

References

1. F London, in "*Superfluids, Macroscopic Theory of Superconductivity*" (Dover, New York, 1950) 31.
2. C J Gorter and H Casimir, *Physica*. **1** (1934) 306.
3. L P Gor'kov, *JETP* (USSR) **36** (1959) 1918, translated in *Soviet. Phys. JETP* **9** (1959) 1364.
4. D Jérome, A Mazaud, M Ribault and K Bechgaard, J. *Phys. Lett*. **41** (1980) L95.
5. J G Bednorz and K A Muller, *Z. Phys*. B: Condensed Matter **64** (1986) 189.
6. A F Hebard, et al., *Nature*. **350** (1992) 600.
7. Nagamatsu, J Nakagawa, N Muranaka, T Zenitani, Y Akimitsu, *Nature*. **410** (2001) 63-64.
8. A Yu Kasumov, et al., *Science*. **284** (1999) 1508.
9. M Kociak, et al., *Phys. Rev. Lett*. **86** (2001) 2416.
10. Z K Tang, Lingyun Zhang, N Wang, X X Zhang, GH Wen, G D Li, J N Wang, C T Chan, Ping Sheng, *Science*. **292** (2001) 2462.
11. A A Abrikosov, *Zh. Eksp. Theor. Fiz*. **32** (1957) 1442; *Soviet Phys. J.E.T.P* **5** (1957) 1174; "Fundamentals of the Theory of Metals" (Elsevier Science Publishers B.V., 1988, Amsterdam, The Netherlands).
12. J D. Livingston, *Phys. Rev*. **129** (1963) 1943.
13. P-G de Gennes, in "Superconductivity of Metals and Alloys" (W. A. Benjamin Inc., New York, 1966) p. 68-69.
14. M Tinkham, in "Introduction to Superconductivity", R E Krieger Ed. (Publishing Co., Malabar, Florida) p. 152.
15. I A Buzdin and A Yu Simonov, *Physica.* B **165-166** (1990) 110.
16. I A Buzdin and A Yu. Simonov, *Physica*. C **175**

(1991) 143.
17. Z Hao, J R Clem, M W McElfresh, L Civale, A P Malozemoff and F Holtzberg. *Phys. Rev*. B **43** (1991) 2844.
18. Z Hao and J R Clem, *Phys. Rev. Lett*. **67** (1991) 2371.
19. R Clem Physica C **153-155** (1988) 50.
20. S Senoussi, *J Phys*. III **2** (1992) 1041.
21. S Senoussi, S Hammond and F Mosbah, in "Studies of high temperature superconductors", A Narlikar Ed., Vol. 14 (Nova Science, Commack, NY, 1995) P. 107.
22. C P Bean: (a) *Phys. Rev. Lett*. **8** (1962) 250 ; (b) *Rev. Mod. Phys*. **36** (1964) 31.
23. S Senoussi, C Aguillon, P Manuel, *Physica* C **175** (1991) 202.
24. S Senoussi, C Aguillon, S Hadjoudj, Physica C **175** (1991) 215.
25. M Oussena, S Senoussi, G Collin, *Europhys. Lett*. **4** (1987) 625.
26. X Su, F Zuo, J A Schlueter, A M Kini and Jack M Williams, *Phys. Rev*. B **58** (1998) R2944.
27. M A Tanatar, V N Laukhin, T Ishiguro, H Ito, T Kondo and G Saito, *Phys. Rev*. B **59** (1999) 3841.
28. M A Tanatar, T Ishiguro, H Ito, M Kubota and G Saito, *Phys. Rev*. B **55** (1997) 12529.
29. T F Stalcup, J S Brooks and R C Haddon, *Phys. Rev*. B **60** (1999) 9309.
30. Y Watanabe, H Sato, T Sasaki and N Toyota, *J. Phys. Soc. Jpn*. **60** (1991) 3608.
31. K Oshima, K Araki, H Yamazaki, H Mori and G Saito, *J. Mag. Mag. Mat*. **90-91** (1990) 785.
32. N Yoneyama1, T Sasaki and N Kobayashi, *J. Phys. Soc. Jpn*. **73** (2004) 1434.
33. M Pinteric, S Tomic, M Prester, D Drobac and K Maki, *Phys. Rev*. B **66** (2002) 174521.
34. H Akutsu, K Saito and M Sorai, *Phys. Rev*. B **61** (2000) 4346.
35. J Müller, M Lang, F Steglich, J A Schlueter, A M Kini and T Sasaki, *Phys. Rev*. B **65** (2002) 144521.
36. P Wzietek et al., *J. Phys. I France* **6** (1996) 2011.
37. A Kawamoto, K Miyagawa and K Kanoda, *Phys. Rev*. B **55** (1997) 14140.
38. S Senoussi and F Pesty, « Studies of high temperature superconductors : Diverse Superconducting Systems and Some Miscellaneous Applications », vol. 37, edited by A. Narlikar (Nova Science Publishers, Huntington, NY, USA, 2001), p. 205-248.
39. M Pinteric, S Tomic and K Maki, *Physica* C **408-410** (2004) 75.
40. A Vainrub, S Vija, E Lippmaa, V Prigodin, R Beha, and M Mehring, *Phys. Rev. Lett*. **69** (1992) 3116.
41. T A Alheiser, R W Giannetta, D D Lawrie, R Prozorov, J A Shlueter, A M Kini and U Geiser, 2006 APS March Meeting (session U38: 1-D Superconductors and Organics)
42. A Aharoni, *J. Appl. Phys*. **87** (2000) 6564.
43. T M Lang et al., *Phys. Rev*. B **46** (1992) 5822.
44. R Clem, *Physica* C **153** (1988) 50.
45. J R Clem, B Bumble, S I Raider, W J Gallagher and Y C Shih, *Phys. Rev*. B **35** (1987) 6637.
46. M V Feigel'man et al., *Phys. Rev. Lett*. **93** (2004) 136402.
47. R M C de Almeida, N Lemke and I A Campbell, Eur. Phys. J. B **18** (2000) 513.
48. A Fierro, A De Candia and A Coniglio, *Phys. Rev*. E **56** (1997) 4990.
49. E A Edwards and P W Anderson, *J. phys.* F **5** (1975) 965.
50. H Mayaffre, P Wzietek, D Jérome, C Lenoir and P Batail, *Europhys. Lett*. **28** (1994) 205.
51. S M De Soto and C P Slichter, A M Kini, H H Wang, U Geiser and J M Williams, *Phys. Rev*. B **52** (1995) 10364.